Nuclear Instruments and Methods in Physics Research A 340 (1994) 524–539
North-Holland

NUCLEAR INSTRUMENTS & METHODS IN PHYSICS RESEARCH
Section A

Auger-free luminescence of the BaF_2:Sr, BaF_2:MgF_2 and CsBr:LiBr crystals under excitation of VUV photons and high-energy electrons

Margarida Mizue Hamada [1]

Department of Physics, Rikkyo University, Nishi-Ikebukuro, Tokyo, 171, Japan

(Received 12 July 1993)

The emission spectrum, the time dependence of the luminescence, the excitation spectrum and the reflectance spectrum have been measured for the pure BaF_2 crystal, the BaF_2.Sr crystals with Sr^{++} concentrations of 2 and 5 mol%, the BaF_2:MgF_2 crystal with a mole mixing ratio of 1:2, and the pure CsBr crystal and the CsBr:LiBr crystal with a mole mixing ratio of 1:1. The measurements have been made by using synchrotron orbital radiation and high-energy electrons produced by gamma-rays. It is shown that the BaF_2, the BaF_2:Sr and the BaF_2:MgF_2 crystals have the Auger-free luminescence having decay times around 0.90 ns. The slow and fast luminescence components of the BaF_2 crystal are suppressed by introduction Sr^{++} and Mg^{++} ions. It is, however, clearly seen that the suppression of the slow component is more effectively occurring than that of the fast component, especially in the BaF_2:MgF_2 crystal. By analyzing the Auger-free luminescence spectrum, it is shown that the valence band widths are 2.7 ± 0.3 eV, 2.7 ± 0.3 eV and 4.2 ± 0.3 eV and the band-gap energies are 11.1 ± 0.3 eV, 11.1 ± 0.4 eV and 11.9 ± 0.4 eV for BaF_2, BaF_2:Sr and BaF_2:MgF_2 crystals, respectively. The introduction of LiBr into CsBr has resulted in a significant enhancement in the luminescence intensity, attaining 40 times larger intensity than that of CsBr crystal at room temperature, due to the suppression of the non-radiative relaxation of the outer-most core holes due to the absorption induced by the Urbach effect. The observations of the increases in the band gap-energy, the exciton energy and the decay time of the CsBr:LiBr crystal compared with those of the CsBr crystal support the argument given in the present study regarding the suppression of the Urbach effect in the CsBr:LiBr crystal. The decay times observed are 0.20 ± 0.05 ns and 0.90 ± 0.06 ns for CsBr and CsBr:LiBr crystals, respectively.

1. Introduction

The interatomic radiative transitions of the electrons from the valence band to the top of the outermost-core band have been investigated in alkali halide and alkaline-earth halide crystals, such as CsCl, CsBr and BaF_2 crystals, by observing the associated luminescence from the crystals [1–13]. These crystals are distinguished from the other crystals of alkali halide and alkaline-earth halide by their band structures in which the energy separation, E_{vc}, between the top of the valence band and the outermost-core band is less than the band-gap energy, E_g. The Auger process is, therefore, energetically prohibited. The luminescence emitted from this type of crystals is called the Auger-free luminescence (AFL) [4] (sometimes called as cross luminescence [3] or radiative core-valence luminescence [8]). Since the decay time of the AFL is order of 1 ns, these crystals have been used as scintillators in such fields like high energy physics [14,15] and nuclear medicine [16,17].

Among these crystals, the pure BaF_2 crystal has been intensively studied [1,3,6,10] and applied to various fields of applications as an excellent scintillating material, because of i) its high density (4.89 g/cm^3), ii) the good time resolution due to the fast component (< 1 ns) appearing in the emission bands around 220 nm and the 195 nm, iii) the relatively large light output compared to conventional scintillators such as BGO, and iv) the high radiation resistance [18]. In addition to the fast component, the BaF_2 crystal has a slow component, which has a maximum emission around 300 nm with a decay time of about 700 ns [5,16–18]. The slow component, however, could cause serious pileup problems with a counting rate higher than 10^6 s^{-1} where the dead time of the detector system due to the slow component becomes comparable to the event intervals [19]. The suppression of the slow component is, therefore, a crucial key to applying this crystal to high counting rate experiments. Although there have been several attempts to reduce the slow component by introduction of rare earth elements into the BaF_2 crys-

[1] On leave from Instituto de Pesquisas Energéticas e Nucleares, IPEN/CNEN-SP, Trav. R no. 400, Cidade Universitária, São Paulo, Brazil.

SSDI 0168-9002(93)E1220-R

tals [17–24], further study for the suppression of the slow component is needed.

The first aim of the present work is to find promising combinations of different alkaline-earth fluoride crystals in which the slow component is highly suppressed. Since the BaF_2 crystal is widely accepted as mentioned above, the author has focused the research on a group of BaF_2-based crystals, synthesizing new combinations of BaF_2 crystals with various alkaline-earth crystals which have not been investigated so far. Newly synthesized in the present work are BaF_2:Sr crystals with Sr^{++} concentrations of 2 mol% and 5 mol%, a BaF_2:MgF_2 crystal with a mole mixing ratio of 1:2. By exciting these crystals with vacuum-ultraviolet (VUV) photons and high-energy electrons, systematic measurements have been made including the emission spectrum, the time dependence of the luminescence, the photo-excitation spectrum and the reflectance spectrum. The results show that the slow component is suppressed by introducing the SrF_2 and MgF_2, together with the suppression of the fast component. However the suppression of the slow component is more effective than that of the fast component. Alexandrov et al. [23] also paid their attention to the combination of BaF_2 with SrF_2. In contrast to our approach, they mixed both crystals in form of powder in which the SrF_2 powder was major component.

Another interesting crystal characterized by the AFL is CsBr, which is known to be the fastest scintillator found so far [5]. The luminescence in the CsBr has been widely studied by several investigators [4,7,9,11, 25,26]. The problem of the crystal is its low AFL intensity at room temperature, which has been ascribed to the non-radiative relaxation process of the outermost-core holes due to the absorption induced by the Urbach effect [26].

The second aim of the present work is to find a way of increasing the luminescence intensity of the CsBr crystal at room temperature by introducing a foreign component. As a first trial a new crystal composed of CsBr and LiBr with a mole mixing ratio of 1:1 was synthesized. Since the band-gap energy of LiBr is larger than that of CsBr [27], it is expected that the band-gap energy and the exciton energy in the CsBr:LiBr crystal are larger than those of the CsBr crystal, thus suppressing the Urbach effect in the crystal. The AFL intensity of the CsBr:LiBr crystal should, therefore, be larger than that of the CsBr crystal. To ascertain this expectation, systematic studies on the AFL of the CsBr and CsBr:LiBr crystals are made by exciting them with VUV photons and high-energy electrons. As expected the experimental result shows 40 times increase in AFL intensity of the CsBr:LiBr crystal compared to that of the CsBr crystal.

The paper is organized as follows: in section 2 the experimental procedure is described; the experimental results are given in section 3; and the discussion is described in section 4. Finally a conclusion is given in section 5.

2. Experimental procedures

2.1. Crystal preparation

Among the crystals investigated, the *first* crystal group of BaF_2, BaF_2:Sr and BaF_2:MgF_2 were obtained from Union Material Inc., Japan. These crystals were grown from starting powder of *suprapure* grade, which were purchased from E. Merck, Germany. In order to study the suppression of the slow component by introduction of the Sr^{++} ions, two BaF_2:Sr crystals having different Sr^{++} concentrations of 2 mol% and 5 mol% were prepared. The mole ratio of MgF_2 mixed to BaF_2 was uniquely determined to be 2:1, in reference to the phase diagram [28].

The *second* crystal group of CsBr and CsBr:LiBr were grown from the melt in accordance with the vertical Bridgman method at Rikkyo University. The starting powder used for crystal growth with purities of 99.90%, was purchased from Metal Gesellschaft K.K., Germany. Prior to the crystal growth, the powder was submitted to the purification process by evacuating it at 300°C for two hours in order to remove residual water. To grow the CsBr crystal, the CsBr powder of 100 g was first placed into a quartz crucible on a furnace stage, and then heated in bromine atmosphere of 200 mmHg up to 650°C. Upon the powder being melt, the crystal was grown with a rate of 0.8 mm/h. To grow a CsBr:LiBr crystal, the CsBr powder and the LiBr powder were mixed together with a mole ratio of 1:1 in a quartz crucible [29]. Two kinds of powder were heated up to 650°C to melt. The melt of the mixture was quickly cooled down to 300°C, which is the optimum temperature for crystal grown of this mixture according to the phase diagram [29]. The CsBr:LiBr crystal was grown with a rate of 0.8 mm/h. The crystal was machined and polished in the dimensions of about $1 \times 1 \times 1$ cm^3.

2.2. Time-resolved spectroscopy

The time characteristics of the luminescence emitted from the crystals as a function of the wavelength, was measured by employing the time-resolved spectroscopy, and irradiating the crystal sample at room temperature with gamma-rays as shown in Fig. 1.

Each crystal was mounted at the site of the entrance slit of a monochromator (Shimadzu Bausch & Lomb), and was irradiated by 511 keV annihilation gamma-rays from a ^{22}Na source (3.7 MBq). The monochromator had a resolving power of 0.1 eV at 5.6

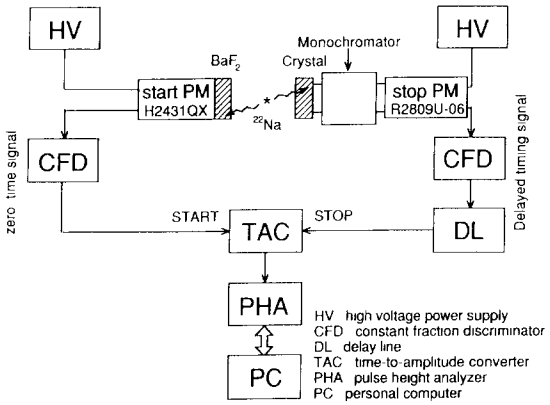

Fig. 1. Block diagram of the electronic system used in time-resolved spectroscopy measurements.

eV. The monochromatized luminescence photons were detected with a UV sensitive microchannel-plate embedded photomultiplier (Hamamatsu Photonics, R2809U-06) which generated delayed timing signals. The correlated 511 keV annihilation gamma-rays from the source were detected with a BaF_2 scintillator (about $2 \times 2 \times 3$ cm^3) coupled to a UV sensitive photomultiplier (Hamamatsu Photonics, H2431QX) to generate zero-time signals.

The zero-time and the delayed timing signals were sent to constant fraction discriminators (ORTEC model 416), and were delivered to a time-to-amplitude converter (ORTEC 437) as start signals and stop signals, respectively. The output pulses from the time-to-amplitude converter were fed into a multichannel analyzer where a luminescence decay curve was accumulated at a given wavelength of the emission. Since the decay curves exhibited several components with different decay times as described in the next section, the range of the time-to-amplitude converter was set to either 50 ns or 10 μs in full scale depending upon the range of interest. Attaining good statistics in the observed decay curves typically required a data accumulation time of 24 h. The data acquired in the multichannel analyzer were sent to a personal computer for further analysis and storage.

2.3. Emission spectrum and light output

The emission spectra of the crystals under investigation were measured by counting the numbers of the photon signals from the R2809U-06 photomultiplier at various wavelengths of luminescence in a common accumulation time. In order to evaluate the contribution of the fast component to the total emission spectra at different wavelengths, the intensity of the fast component observed at a given wavelength was determined by summing the counts recorded in the decay curve from its time origin to 4 ns. The measured emission spectra were corrected for the spectral response of the detection system.

The relative light outputs of the fast component of the BaF_2-based crystals under irradiation of 662 keV gamma-rays from a ^{137}Cs source were measured with a UV sensitive quartz photomultiplier (Hamamatsu Photonics, R1668). A silicon compound, 600000 cSt in viscosity (General Electric, Viscasil), was used to assure the optical contact between the photomultiplier window and the crystal. All the surfaces of the crystal were uniformly wrapped with Teflon tape to improve the reflectivity, except for the one in contact with the photomultiplier window. The output signals from the photomultiplier were shaped with a resistance capacitance (RC) network having RC clipping time constant of about 5 ns. After amplified with a fast pre-amplifier (ORTEC model 9301) and shaped with a main amplifier (ORTEC model 410), the output pulses were submitted to a multichannel analyzer for pulse height analysis.

2.4. Emission, photo-excitation and reflectance measurement with SOR excitation

Synchrotron orbital radiation (SOR) at the Institute for Solid State Physics, Tokyo University, was employed as an excitation light source to investigate the spectral characteristics of the AFL of the crystals. The VUV photons from SOR were monochromatized with a 1 m Seya-Namioka monochromator. The energy resolution of the monochromator was about 0.8 nm with a slit width of 100 μm, corresponding to 0.02 and 0.12 eV at photon energies of 6 and 14 eV, respectively. A surface of the crystal to be studied was exposed to the monochromatized VUV photons with a normal angle. The luminescence emitted from the crystals was viewed at 70° with respect to the exciting light axis, and was focused with a quartz lens on the entrance slit of a second monochromator (Shimadzu Bausch & Lomb). The band width of the second monochromator was fixed to 0.1 at 5.6 eV. The photon signals monochromatized with the second monochromator were detected with a quartz window photomultiplier (Hamamatsu Photonics, R585). The photo-excitation spectrum was measured as a function of the excitation photon energy. The relative AFL intensities for CsBr-based crystals were measured under irradiation of VUV photons.

The intensity of the reflected VUV photons at the crystal surface was also measured to obtain complementary information to the photo-excitation spectrum. The reflected photons with an energy ranging from 6 to 25 eV were detected with a photomultiplier (Hamamatsu Photonics, R105) having a viewing angle of 50° with respect to the exciting light axis. In order to make

the photomultiplier to be sensitive to VUV photons, the window was coated with a thin layer of sodium salicylate, which converts VUV photons into visible ones with an emission spectrum peaking around 420 nm.

3. Results

3.1. BaF_2, BaF_2:Sr and BaF_2:MgF_2

3.1.1. Total emission spectra observed under high-energy electron excitation

Fig. 2 shows the emission spectra measured for the BaF_2, the BaF_2:Sr (5%) and the BaF_2:MgF_2 crystals at room temperature under the excitation of high-energy electrons generated by 511 keV annihilation gamma-rays. The spectrum for the BaF_2:Sr (2%) crystal is not displayed in this figure, since it shows a nearly identical feature to that of the BaF_2:Sr (5%) crystal. All the spectra are normalized in such a way that they show the same intensities at their maximum emission.

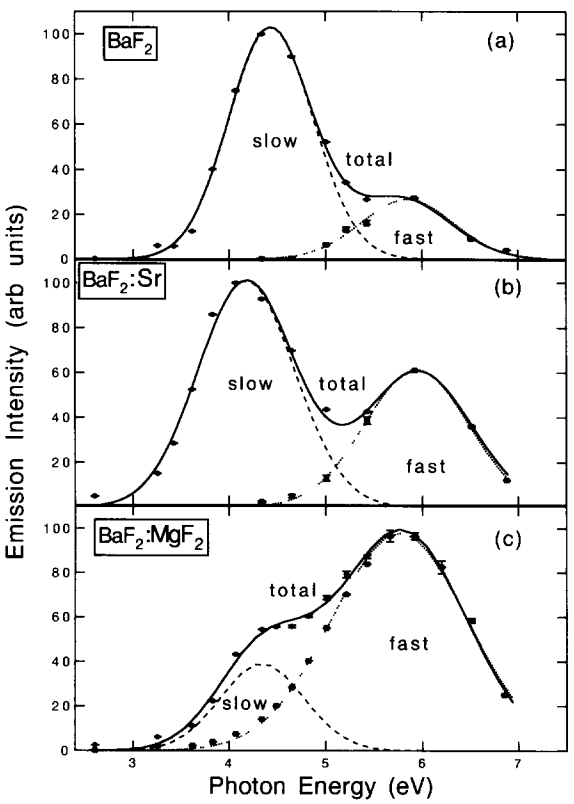

Fig. 2. Emission spectra of BaF_2, BaF_2:Sr (5%) and BaF_2:MgF_2 under high-energy excitation. Solid curve: total emission spectra. Dotted curve: fast emission spectra. Dashed curve: slow emission spectra.

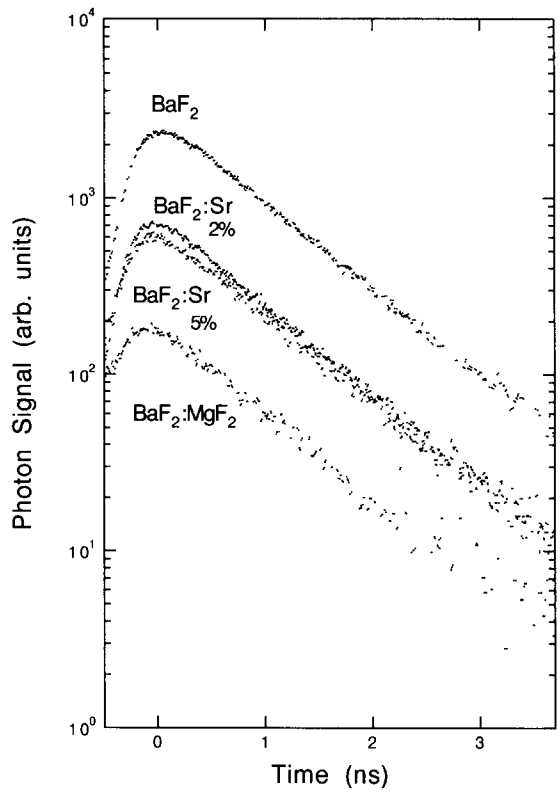

Fig. 3. Decay curves of the HEL band in BaF_2, BaF_2:Sr (2%), BaF_2:Sr (5%) and BaF_2:MgF_2 measured under high energy electron excitation.

Double peak structures are commonly recognized in all spectra measured. The peaks are locating at 5.9 and 4.2 eV for the BaF_2 and the BaF_2:Sr (5%) crystals [30], while they are at 5.7 and 4.2 eV for the BaF_2:MgF_2 crystal. Since all the spectra measured show the double-peak structure, the peaks appearing at higher and lower energy regions are, hereafter, referred to as the high-energy luminescence (HEL) band and the low-energy luminescence (LEL) band, respectively. The emission spectrum of a pure MgF_2 crystal is also measured, however, there is no emission band detected whose intensity exceeds higher than 10^{-3} of the BaF_2:MgF_2 crystal emission. It should be noticed here that the intensity of the HEL band for the BaF_2:MgF_2 crystal is larger than that of the LEL band. This is quite contrary to the case of the BaF_2 and the BaF_2:Sr crystals in which the LEL bands are dominant.

3.1.2. Decay curves

Fig. 3 shows the decay curves measured for the HEL bands in the BaF_2, BaF_2:Sr (2%), the BaF_2:Sr (5%) and the BaF_2:MgF_2 crystals. All curves show single-exponential decays with a common decay time of about 0.9 ns. No appreciable difference was observed

Table 1
Decay times and relative light outputs of the fast component The ratios F/S of the fast component intensity to the slow component intensity are also indicated. Experimental uncertainties are 15% in the last two columns

Crystal	Decay time [ns]	Relative light output [%]	F/S
BaF_2	0.90 ± 0.06	100	0.28
BaF_2:Sr (2%)	0.89 ± 0.05	41	0.48
BaF_2:Sr (5%)	0.87 ± 0.05	27	0.60
BaF_2:MgF_2	0.89 ± 0.04	22	2.70

Table 2
Decay times for the slow component and the ratios I_1/I_2 of the intensity of the τ_1 decay component to that of the τ_2 decay component. The relative light outputs of the slow component are also summarized

Crystal	τ_1 [ns]	τ_2 [ns]	I_1/I_2	Relative light output [%]
BaF_2	330 ± 30	670 ± 60	0.44 ± 0.10	100
BaF_2·Sr (2%)	300 ± 40	680 ± 70	0.30 ± 0.06	23
BaF_2·Sr (5%)	150 ± 20	700 ± 70	0.15 ± 0.03	13
BaF_2.MgF_2				2

in the time dependence among the decay curves. The measured decay times are summarized in Table 1.

Fig. 4 shows the decay curves measured for the LEL bands in the BaF_2, the BaF_2:Sr (2%) and the BaF_2:Sr (5%) crystals. As can be seen from Fig. 4, at least three decay components exist in these curves. Although the intensity is considerably small compared with the other components, an extremely fast component is clearly recognized as a spike near the time origin with a decay time of about 1 ns. Disregarding the fast component, the observed decay curves are fitted to a two-exponential function with decay time constants of τ_1 and τ_2, i.e., $(I_1/\tau_1)\exp(-t/\tau_1) + (I_2/\tau_2)\exp(-t/\tau_2)$. Table 2 summarizes the fitted values of τ_1, τ_2 and the relative intensity I_1/I_2. Although none of the crystals shows any differences in τ_2 from that of the BaF_2, the determined value of τ_1 for the BaF_2:Sr (5%) crystal is found to be nearly a half of that of BaF_2 crystal. The decay curve for the LEL band in the BaF_2:MgF_2 crystal could not be obtained, because emission intensity is not as intense as those in the BaF_2 and the BaF_2:Sr crystals.

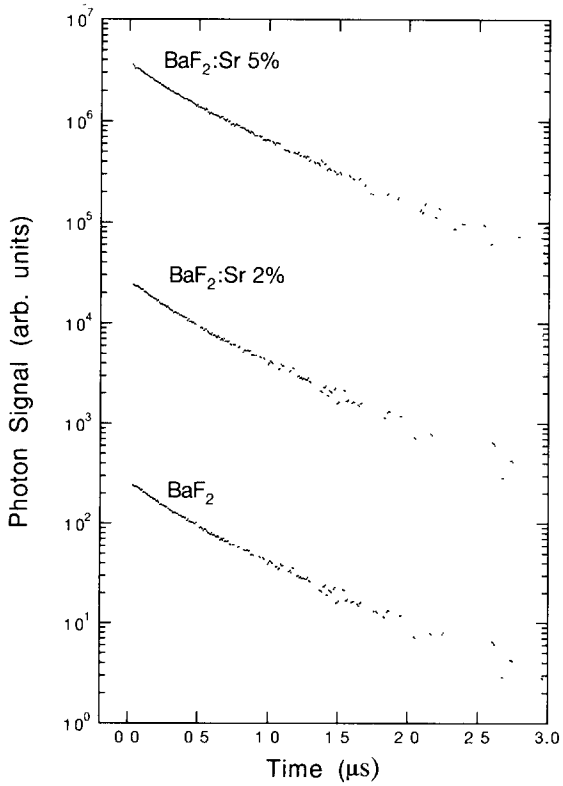

Fig. 4. Decay curves of the LEL band in BaF_2, BaF_2:Sr (2%), BaF_2 Sr (5%) measured under high-energy excitation.

3.1.3. Emission spectra for the fast and the slow components

In Fig. 2, the dotted lines indicate the intensity of the fast components observed in the BaF_2, the BaF_2:Sr and the BaF_2:MgF_2 crystals as a function of the luminescence photon energy. These time-resolved emission spectra are superimposed to the total emission spectra in such a way that both spectra coincide at the peaks in the higher energy regions, since the fast components are dominant there as reported above. The time-resolved spectra for the slow components are obtained by subtracting the fast component spectrum from the total emission spectra. The slow component emission spectra thus obtained are shown by dashed curves in Fig. 2. After separating the total emission spectra into two independent components, it can be seen that the HEL bands distribute from 4.2 to 6.9 eV in the BaF_2 and the BaF_2:Sr crystals, while it distributes from 3.2 to 7.4 eV for the BaF_2:MgF_2 crystal. It should be noted here that the spectrum width (4.2 eV) of the fast component for the BaF_2:MgF_2 crystal is larger than those (2.7 eV) for the BaF_2 and the BaF_2:Sr crystals.

3.1.4. Light output for the fast components

Under the excitation of high-energy electrons generated by 662 keV gamma-rays, the light output of the fast component, relative to that for the BaF_2 crystals, is measured to be 0.41, 0.27 and 0.22 for the BaF_2:Sr (2%), the BaF_2:Sr (5%) and the BaF_2:MgF_2 crystals,

respectively, as listed in Table 1. Fig. 5 compares the emission spectra of the BaF_2, the BaF_2:Sr (2%), the BaF_2:Sr (5%) and the BaF_2:MgF_2 crystals under high-energy electron excitation generated by 511 keV gamma-rays. In this figure, the intensities at the maximum values of the HEL were scaled by using their relative light output ratios indicated above. As can be seen, the HEL (fast component) and the LEL (slow component) bands decrease with the addition of Sr^{++} and Mg^{++}. Table 1 also compiles the intensity ratios of the fast components to the slow components in these crystals. The light output of the slow component, relative to that for the BaF_2 crystals, is summarized in Table 2. As the BaF_2:MgF_2 crystal clearly demonstrates the slow component is more effectively suppressed than the fast component.

3.1.5. Emission induced by VUV excitation

Fig. 6 shows the emission spectra of the BaF_2, the BaF_2:Sr (5%) and the BaF_2:MgF_2 crystals at room temperature irradiated with 21.7 eV photons which can excite the outermost Ba^{++} 5p core band. As in the case of high-energy electron excitation, the HEL and the LEL bands have the maximum emission around 5.9

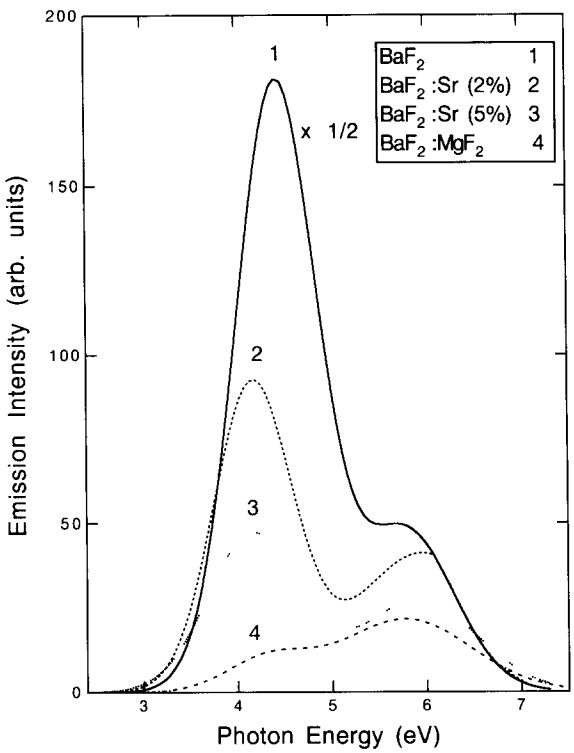

Fig. 5. Emission spectra of the BaF_2, BaF_2:Sr (2%), BaF_2:Sr (5%) and BaF_2:MgF_2. The intensity at the maximum values of HEL band are adjusted in accordance with their relative light yield ratios.

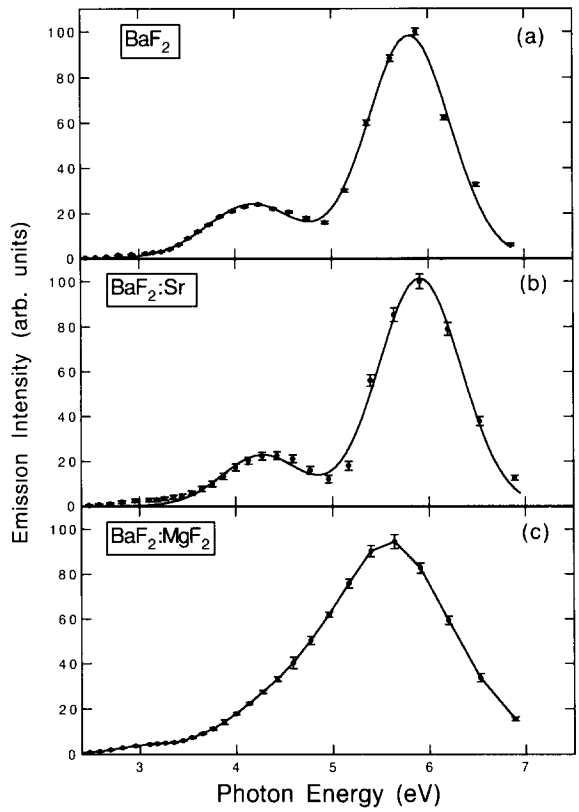

Fig. 6. Emission spectra of BaF_2, BaF_2:Sr (5%) and BaF_2:MgF_2 measured under 21.7 eV photon-excitation.

and 4.1 eV, respectively, in the BaF_2 and the BaF_2:Sr crystals. In contrast to the high-energy electron excitation, however, the HEL band is dominant for the BaF_2:Sr and the BaF_2 crystals. The BaF_2:MgF_2 crystal has a single broad band having a maximum around 5.7 eV as shown in Fig. 6c.

3.1.6. Photo-excitation spectra and reflectance spectra

Figs. 7a, 7b and 7c show the measured photo-excitation spectra of the fast and the slow components of the BaF_2, the BaF_2:Sr (5%) and the BaF_2:MgF_2 crystals at room temperature. The threshold energies, E_{th}, above which the fast component appears are determined to be 18.0 ± 0.2 eV for both the BaF_2 and the BaF_2:Sr crystals, while E_{th} is determined to be 19.3 ± 0.2 eV for the BaF_2:MgF_2 crystal from Fig. 7. The slow component for the BaF_2 and the BaF_2:Sr crystals is found to be excited abundantly around the excitation photon energy of exciton excitation and of valence-band excitation. For the BaF_2:MgF_2 crystal photo-excitation spectrum of the slow component has a fine single peak at 10 eV.

The reflectance spectra measured for the BaF_2 and the BaF_2:Sr (5%) crystals at room temperature are

displayed in Figs. 7a and 7b. For the BaF_2 crystal, there are three major peaks observed in the reflectance spectrum, which are assigned to the core exciton energy (A and B) and the exciton energy (Γ), and are in good agreement with those reported by Rubloff [31]. The BaF_2:Sr (5%) crystal does not show any particular difference in reflectance spectrum from the BaF_2 crystal. An intense peak was found at 9.8 ± 0.1 eV in the exciton energy region and two strong peaks at 17.1 ± 0.1 eV and 19.8 ± 0.1 eV were observed in the core exciton region. In the BaF_2:MgF_2, two peaks at 10.0 ± 0.3 eV and 11.0 ± 0.4 eV are observed in the exciton energy region. A broad band locating around 18.6 ± 0.3 eV and is observed in the core exciton region.

3.2. CsBr:LiBr and CsBr

3.2.1. Total emission spectra observed under high-energy electron excitation

Fig. 8a displays the time-resolved emission spectrum of the CsBr crystal. As can be seen, a single continuous emission band is found, with the maximum emission at 5.3 eV. This band consists of a fast component with a decay time of 0.2 ns as described later. There is a minor shoulder-like structure observed at 4.1 eV as well. Due to the low emission intensity of the CsBr crystal at room temperature, the present spectroscopic system was incapable of providing decent results on the total emission spectrum of the crystal. Mixing LiBr into the CsBr, however, changed the monotonous spectrum into a rather varied one as shown in Fig. 8b. The total emission spectrum of the CsBr:LiBr crystal observed at room temperature under the high-energy electron excitation has a peak at 3.6 eV in the LEL region and a peak at 4.4 eV together with a minor one at 5.6 eV in the HEL region. The intensity of the 5.6 eV luminescence band is about 80 times weaker than that of the 4.4 eV luminescence band.

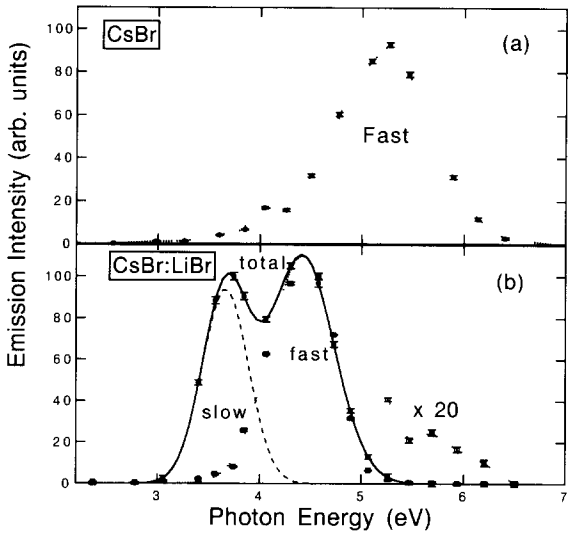

Fig. 8. Emission spectra of CsBr:LiBr and CsBr under high-energy excitation at room temperature. Solid curve: total emission spectra. Dotted curve: fast emission spectra. Dashed curve: slow emission spectra.

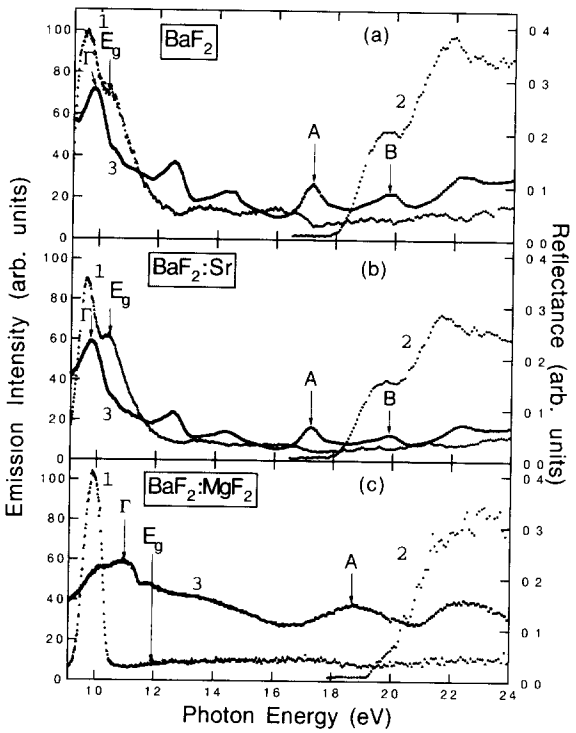

Fig. 7. Excitation spectra for 5.9 eV band (BaF_2), 5.9 eV band (BaF_2:Sr) and 5.7 eV band (BaF_2:MgF_2) are shown by dotted lines labeled 2. Excitation spectra for the 4.2 eV band from BaF_2, BaF_2:Sr and BaF_2:MgF_2 are shown by lines labeled 1. Reflectance spectra are shown by lines labeled 3. The peak positions of the excitons are indicated by Γ and those for the core excitons by A and B. The band gap positions are also indicated by E_g.

3.2.2. Decay curves

The decay curve for the HEL (4.4 eV) band in the CsBr:LiBr crystal manifests a single exponential decay with a fitted decay time of 0.90 ± 0.06 ns as shown in Fig. 9. The decay profile for the 5.6 eV luminescence band is almost identical to that for the 4.4 eV luminescence band. The decay curve for the LEL band (3.6 eV) could not be obtained with the present experimental apparatus because of its low luminescence intensity and long decay time of more than 100 ns. As shown in Fig. 9, the decay curve observed for the 5.3 eV band in the CsBr crystal shows also a single exponential decay with a fitted decay time of 0.20 ± 0.05 ns. The deter-

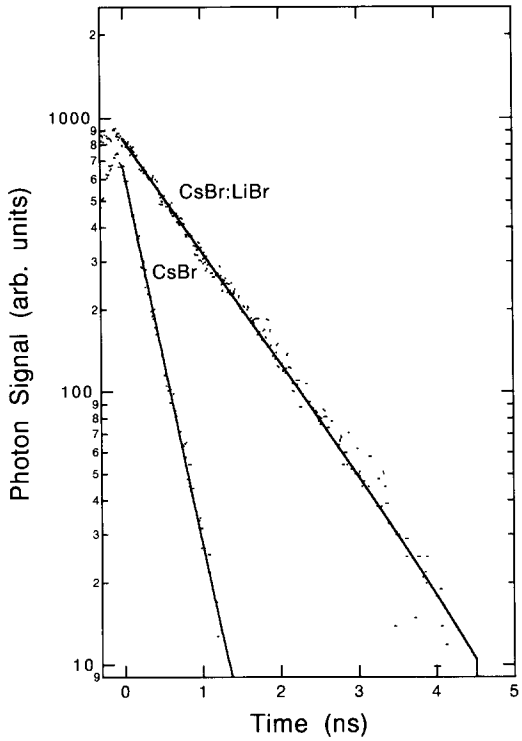

Fig. 9. Decay curves of the HEL band (5.6 eV) in CsBr:LiBr and (5.3 eV) in CsBr.

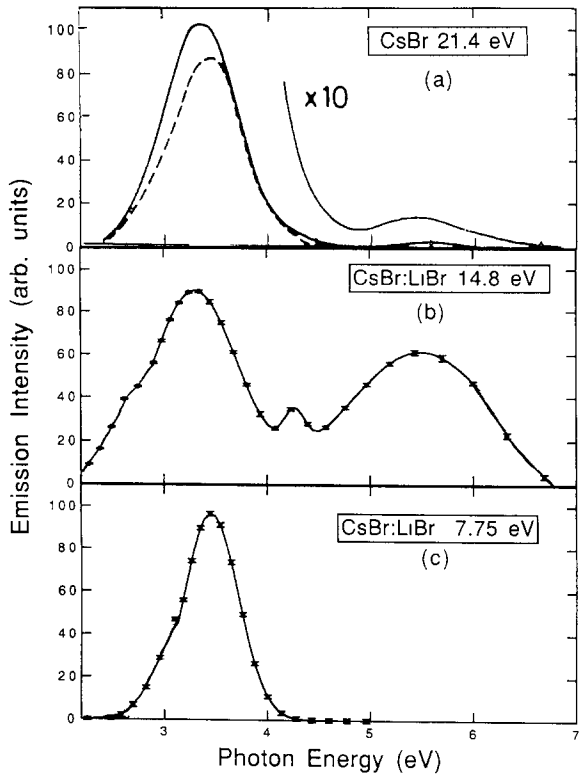

Fig. 10. Emission spectra of CsBr (ref. [4]) and CsBr:LiBr measured under 14.8 eV photo-excitation and 7.75 eV photo-excitation at room temperature.

mined decay time for the 4.1 eV luminescence band does not indicate any difference from that of the 5.3 eV band. The fitted decay times for both crystals are listed in Table 3.

3.2.3. Emission spectra for the fast and slow components

The time resolved emission spectrum for the fast (nanosecond) component observed in the CsBr:LiBr crystal is shown in Fig. 8b by the dotted curve. In this spectrum, the maximum emission intensity at the photon energy of 4.4 eV is normalized to that of the total emission spectrum at that energy. The spectrum of the slow component is obtained by subtracting the fast component spectrum from the total emission spectrum. The slow component spectrum thus determined is shown by the dashed curve. It can be seen from this figure that the HEL and the LEL bands distribute from 3.6 to 6.6 eV and from 3.0 to 4.2 eV, respectively.

Table 3
Decay times for the fast component in CsBr and CsBr:LiBr crystals and the relative luminescence intensities for the fast component. The experimental uncertainties are 20% in the last two columns

Crystal	Peak position of AF emissions bands [eV]	τ [ns]	Relative intensity [%]	
			Room temperature	Liquid nitrogen temperature
CsBr	5.3	0.20 ± 0.05	1	100
	4.1	0.23 ± 0.04		
CsBr:LiBr	5.6	0.90 ± 0.06	40	200
	4.4	0.86 ± 0.05		

3.2.4. Emission spectra under VUV excitation

Figs. 10b and 10c show the observed emission spectra of the CsBr:LiBr crystal observed at room temperature under the outermost Cs^+5p core band excitation with 14.8 eV VUV photons and the valence band excitation with 7.75 eV VUV photons, respectively. Three emission bands are observed at 5.5, 4.3, 3.4 eV under the core band excitation. The 3.4 eV luminescence band exhibits a shoulder on the lower energy wing at 2.8 eV. Under the valence band excitation a LEL band at 3.5 eV is observed as a dominant emission. It should be noticed here that the spectral structure and the intensity ratios among these three peaks are entirely different from those under the high-energy electron excitation as shown in Fig. 8b. The emission

spectra of the CsBr crystal observed under the core band excitation and the valence band excitation are presented in Fig. 10a for reference as reported in ref. [4]. The SOR intensity available in the present study was, unfortunately, insufficient to perform the emission spectrum measurements of the CsBr crystal due to the low luminescence intensity of this crystal.

Figs. 11a and 11b show the emission spectra of the CsBr and the CsBr:LiBr crystals cooled at liquid nitrogen temperature. Three bands having the maximum emissions at 5.4, 3.8 and 2.8 eV are clearly observed in the CsBr:LiBr crystal, while two bands peaking at 5.4 and 3.8 eV with a shoulder on the lower energy wing at 2.9 eV are observed in the CsBr crystal, being in good agreement to ref. [11]. The intensity of the 5.4 eV luminescence band exceeds those of the 3.8 and 2.8 eV bands, which is quite contrary to the results at room temperature.

3.2.5. Luminescence intensity for the fast components

The intensities of the fast components in the CsBr:LiBr and the CsBr crystals are measured at liquid nitrogen temperature as well as at room temperature by using 14.8 eV photons. At room temperature, there is no luminescence detected in the CsBr crystal in the present study. Cooling the CsBr crystal down to liquid nitrogen temperature results in a substantial increase of the fast component. This result is consistent to the other studies done so far in which the intensity at room temperature has been reported to be less than 1/100 of that at liquid nitrogen temperature [5,11]. It is also found that the measured AFL intensity of the CsBr:LiBr crystal at room temperature is 2.5 times

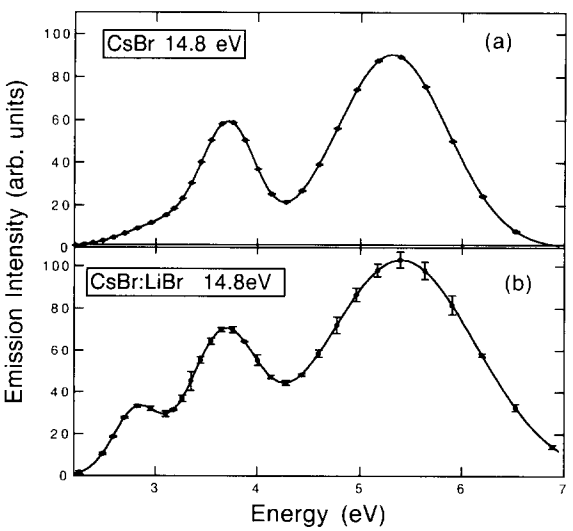

Fig. 11. Emission spectra of CsBr and CsBr:LiBr measured under 14.8 eV photo-excitation at liquid nitrogen temperature.

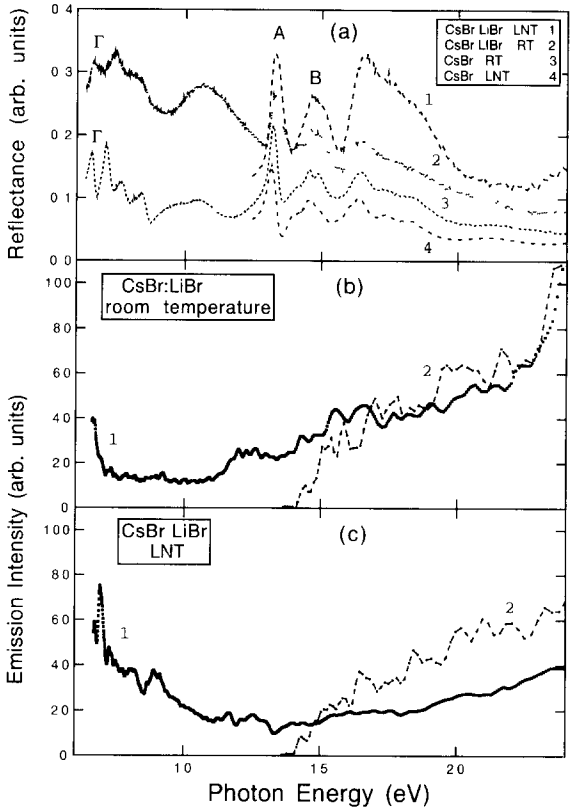

Fig. 12. Reflectance spectra (a) for CsBr and CsBr:LiBr measured at room temperature and liquid nitrogen temperature. Excitation spectra for the 3.4 eV band labeled 1 and the 5.5 eV band labeled 2 from CsBr:LiBr crystal measured at room (b) and liquid nitrogen (c) temperatures.

lower than the measured AFL intensity of the CsBr crystal at liquid nitrogen temperature. In reference to these facts, one could state that the AFL intensity of the CsBr:LiBr crystal at room temperature is 40 times larger than that in pure CsBr. At liquid nitrogen temperature, the measured AFL intensity of the CsBr:LiBr crystal is two times larger than that of the CsBr crystal. These results are summarized in Table 3.

3.2.6. Photo-excitation spectra and reflectance spectra

Figs. 12b and 12c show the photo-excitation spectra measured for the fast (5.5 eV) and slow (3.4 eV) components of the CsBr:LiBr crystal at room and liquid nitrogen temperatures. The photo-excitation spectrum for the 4.3 eV luminescence band is not included, since it is nearly identical to that for the 5.5 eV luminescence band. The threshold energy E_{th} is measured to be 14.1 ± 0.1 eV at room and liquid nitrogen temperatures. The 3.4 eV luminescence band is found to be efficiently excited at room and liquid nitrogen

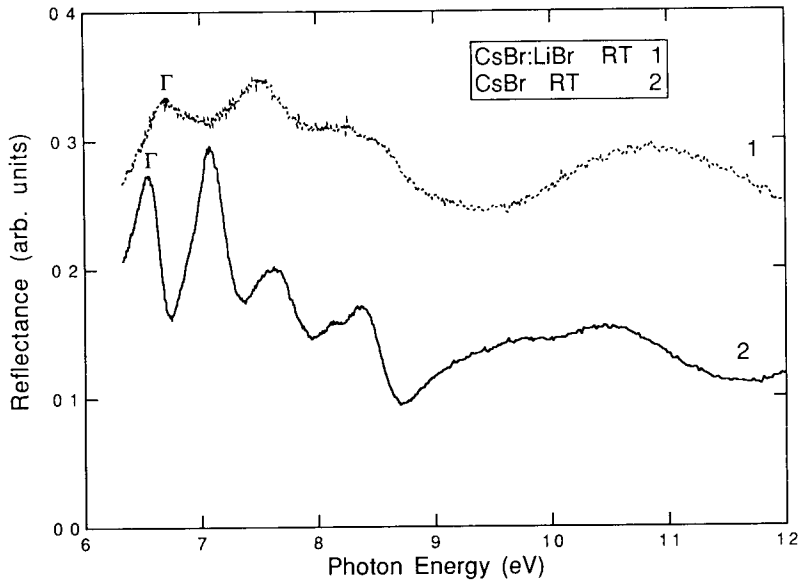

Fig. 13. Reflectance spectra expanded in the valence exciton region for CsBr and CsBr:LiBr measured at room temperature.

temperatures around 7.0 eV, which corresponds to the fundamental absorption edge of the crystal.

Fig. 12a shows the reflectance spectra for the CsBr and the CsBr:LiBr crystals at room temperature. Fig. 13 shows the reflectance spectra expanded in the valence exciton region for the CsBr and the CsBr:LiBr crystals. The reflectance spectrum measured in this study for the CsBr crystal at room temperature is in good agreement with that reported by Rubloff [31]. In the valence exciton region, the lowest energy peak, denoted as Γ, is observed at 6.55 ± 0.02 eV in the CsBr crystal. On the other hand, the corresponding peak is observed at 6.70 ± 0.03 eV in the CsBr:LiBr crystal. In the high-energy region, the peaks are observed at 13.3 ± 0.1 eV and 14.6 ± 0.2 eV in both crystals.

4. Discussion

4.1. Auger-free luminescence

Band structure calculations [32,33] for ionic crystals show that the conduction band consists of the excited s and d states of the positive ions and the valence band filled with p states of the negative ions. Below the valence band, there is an outermost-core band filled with p states of positive ions. Fig. 14 shows schematic energy diagrams, illustrating the AFL and Auger electron emission. When the excitation energy deposited in an ionic crystal by energetic electrons or by VUV photons is high enough to ionize the outermost-core band, there will be created electrons in the conduction band and holes in the outermost-core band in the ionic crystals. Then the valence band electrons recombine with holes in the outermost-core band. The consequence of the recombination process is strongly dependent upon the amount of the energy released during the process which is well represented by the energy difference E_{vc} between the tops of the valence band and the outermost-core band. In case E_{vc} is smaller than the band gap-energy E_g, Auger electron emission is energetically impossible. Then the outermost-core holes are free from the Auger electron emission and combine with the valence electron. The recombination process will, therefore, result in the emission of radia-

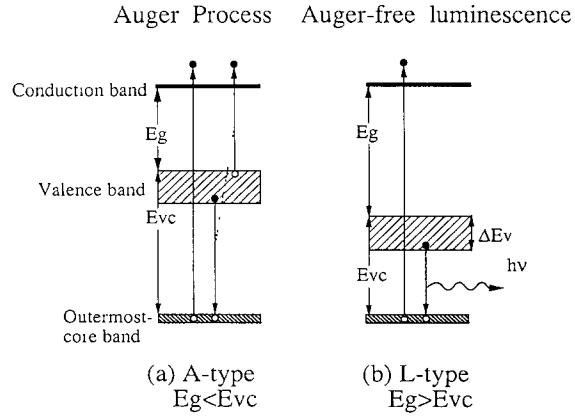

Fig. 14. Schematic energy diagrams illustrating the AFL and Auger electron emission.

Table 4
Summary of the parameters relevant to AF luminescence and the peak position of emission band for the BaF_2-based crystals measured at room temperature. All values are in eV

Crystal	Experiment						Calculation		
	E_{th}	E_g	E_{peak}	E_{max} E_{vc}	E_{min}	Spectrum width $E_{max}-E_{min}$ ΔE_v	Valence band width ΔE_v^p	E_{max} E_{vc}^p	E_{min} $E_{vc}^p-\Delta E_v^p$
BaF_2	18.0 ± 0.1	11.1 ± 0.3	5.9	6.9 ± 03 [h]	4.2 ± 0.1	2.7 ± 0.3	3.4 ± 0.2 [f]	7.2 ± 0.2 [f]	3.8 ± 0.3
	18.23 [a]	10.94 [a]		$7\,3\pm0.1$ [d]	$4.0\pm0\,2$ [d]	3.3 ± 0.2 [d]	2.9 ± 0.2 [g]	7.3 ± 0.2 [g]	4.4 ± 0.3
	10.0 ± 0.2 [b]	10.5 ± 0.2 [c]		6.8 [e]	4.3 [e]	$2\,5$ [e]			
BaF_2:Sr (2%)	18.0 ± 0.2	11.1 ± 0.4	5.9	6.9 ± 0.3 [h]	4.2 ± 0.1	2.7 ± 0.3			
BaF_2:Sr (5%)	18.0 ± 0.2	$11\,1\pm0.4$	5.9	6.9 ± 0.3 [h]	4.2 ± 0.1	$2\,7\pm0.3$			
BaF_2-MgF_2	19.3 ± 0.2	$11\,9\pm0.4$	5.7	7.4 ± 0.3 [h]	3.2 ± 0.1	4.2 ± 0.3			

[a] Ref. [25]. [b] Ref. [10]. [c] Ref. [40] [d] Ref. [3]. [e] Ref. [5]. [f] Ref. [34]. [g] Ref. [41]
[h] The E_{max} values are a reasonable guess from Fig. 2, because of no sensitivity of the present detection system in the spectral region above 6.9 eV.

tion, and is called Auger free luminescence as explained before. Those crystals which satisfy the condition of $E_g > E_{vc}$ are referred to as type L crystals. In case $E_g < E_{vc}$, on the other hand, the Auger process becomes dominant, reducing the luminescence intensity significantly. This type of crystals is referred to as type A crystals. BaF_2 crystal is known as a typical example of the type L, while the SrF_2 and the MgF_2 crystals are categorized in the type A.

Since the AFL is associated with the creation of the holes in the outermost core band, there exists the threshold energy E_{th}, corresponding to the energy of $E_g + E_{vc}$ in the photo-excitation spectrum, above which the excitation energy becomes sufficient to ionize the outermost core band. One can, therefore, obtain the value of $E_g + E_{vc}$ by determining E_{th}, from the photo-excitation spectrum observed.

If the lattice relaxation is negligible, the emission spectrum for the AFL distributes in the region of $E_{vc} - \Delta E_v < h\nu < E_{vc}$ [3,11,25]. Here, ΔE_v denotes the width of the valence band. The values of E_{vc} and ΔE_v can be experimentally determined from the maximum photon energy E_{max} and the width $E_{max} - E_{min}$ of the emission spectrum, respectively, where E_{min} denotes the minimum photon energy of the emission spectrum. By using the values of E_{th} and E_{vc}, the values of E_g for the crystals investigated in the present work have been determined and are listed in Tables 4 and 5.

4.2. BaF_2-based crystals

4.2.1. BaF_2:Sr

Since there are remarkable similarities in the observed reflection spectrum between the BaF_2:Sr and the BaF_2 crystals, it is assumed that the first peak (Γ) at 9.8 ± 0.1 eV and the peak at 17.1 ± 0.1 eV of the BaF_2:Sr crystal correspond to the exciton and the $Ba^{++}5p$ core exciton creations, respectively, as Rubloff ascribed in the case of BaF_2 [31].

As reported in the previous section, there is no difference observed between the BaF_2 and the BaF_2:Sr crystals in the threshold energy in the photo-excitation spectrum for the fast component. This observation leads us to ascribe the fast component to the AFL associated with the radiative recombination of the valence electrons with the holes in the $Ba^{++}5p$ band as

Table 5
Summary of the parameters relevant to AF luminescence and the peak positon of emission band for CsBr and CsBr:LiBr crystals measured at room temperature All values are in eV

Crystal	Experiment						Calculation		
	E_{th}	E_g	E_{peak}	E_{max} E_{vc}	E_{min}	Spectrum width $E_{max}-E_{min}$ ΔE_v	Valence band width ΔE_v^p	E_{max} E_{vc}^p	E_{min} $E_{vc}^p-\Delta E_v^p$
CsBr	13.82 [a]	7 16 [a]	5.3, 4.1	6.6 ± 0.1	3.2 ± 0.1	3.4 ± 0.2	$2\,1+0.2$ [d]	$6.6+0.2$ [d]	4.5 ± 0.3 [d]
	$13.1\ \pm0.2$ [b]			6.2 ± 0.3 [b]	$4\,4+0.1$ [b]	1.8 ± 0.3 [b]	3.0 ± 0.1 [e]	7.3 ± 0.1 [c]	4.3 ± 0.1 [e]
	$14.01\pm0\,1$ [c]				4.5 ± 0.1 [c]	2.0 ± 0.1 [c]			
CsBr–LiBr	$14.1\ \pm0.1$	7.5 ± 0.1	5.6, 4.4	6.6 ± 0.1	3.6 ± 0.1	3.0 ± 0.1			

[a] Ref. [25]. [b] Ref. [4]. [c] Ref. [3] [d] Ref. [39]. [e] Ref. [36].

for BaF_2 crystal. It seems also quite natural to attribute the slow component to the radiative decay of the self-trapped excitons formed by the excitons or electron–hole pairs, since the time characteristic is nearly the same as that of the BaF_2 crystal and it is excited around the excitation photon energy of exciton excitation and of valence-band excitation.

According to the discussion in the section of 4.1, the energy of the emitted photons, $h\nu$, released in the AFL mechanism should be in the range of $E_{vc} - \Delta E_v < h\nu < E_{vc}$. By using the reported values of both E_{vc} and ΔE_v for BaF_2 crystal, which were obtained from photoelectron spectroscopy [34], one can determine the range to be 3.8 eV $< h\nu <$ 7.2 eV for BaF_2 crystal. The energy range estimated in this way is consistent with the one determined from the maximum and minimum energies of the fast emission spectrum from BaF_2:Sr crystal as well as BaF_2 crystal.

Since all the parameters characterizing the AFL for BaF_2:Sr crystal are almost equal to those for the BaF_2 crystal, one can conclude that introduction of SrF_2 into BaF_2 has little effect in the resultant band structure, except for the mechanism controlling the relative light output and the intensity ratio between the fast and slow components in the crystal. The decrease of the fast component could be explained by the fact that the $Sr^{++}4p$ core band which has an excitation energy of 24 eV [34] can be excited as well as the $Ba^{++}5p$ core under the high-energy electron excitation. With raising the Sr^{++} ions concentration, the number of the holes produced in the $Sr^{++}4p$ core band increases and that in the $Ba^{++}5p$ core band decreases. As the SrF_2 crystal is the type A crystal, the holes generated in the $Sr^{++}4p$ core band can relax non-radiatively, thus reducing the intensity of the fast component [5,6]. This explanation has, however, a difficulty in clarifying the mechanism by which only 2–5% of Sr^{++} ions concentration in the BaF_2 crystal can decrease nearly 60% of the entire luminescence intensity.

It is known that the SrF_2 crystal has the broad luminescence band peaking around 4.3 eV, which corresponds to the slow component with a decay time of 900 ns [5]. This slow component is attributed to the radiative decay of self-trapped excitons produced by the recombination process of the electrons in the conduction band with the holes in the valence band [35]. Because the band gap-energy (11.6 eV) of SrF_2 [34] is almost the same as that (11.0 eV) of BaF_2 [34], one could expect that the number of electron–hole pairs produced in the BaF_2 crystal doped 2–5% Sr^{++} ions should not manifest any significant difference from that in a pure BaF_2 crystal. The intensity of the slow component for the BaF_2:Sr crystal should, therefore, be as strong as that for the BaF_2 crystal, unless the introduction of Sr^{++} ions into the BaF_2 crystal has a substantial effect on the efficiency of the self-trapped exciton luminescence. The decrease in the luminescence intensity for the slow component was, however, clearly observed in the present study. This result, therefore, suggests that a considerable decrease in the efficiency for the self-trapped exciton luminescence has been induced by introduction of Sr^{++} ions. Since the decay times τ_1 and τ_2 of the slow component of the BaF_2:Sr crystal are almost the same as those in the BaF_2 crystal, it can be concluded that the introduction of Sr^{++} ions does not affect the decay rate of the self-trapped excitons. In this argument the I_1 component can be neglected, since it contributes only 15% to the total intensity even in the BaF_2:Sr (5%) crystals. The probable explanation for the decrease in the intensity is, therefore, that the Sr^{++} ions are existing as electron trapping centers which prevent the electrons from recombining with the holes, resulting in the reduction of the number of the self-trapped excitons. Schotanus et al. have reported a similar decrease in the intensity of the slow component in a La^{+++} doped BaF_2 crystal, and have interpreted it by the same mechanism [17].

In the BaF_2 and the BaF_2:Sr crystals, an incident photon with the energy higher than E_{th} creates an outermost-core hole accompanied by a photo-electron. After the emission of AFL involving this outermost-core hole and an electron in the valence band, it remains a hole in the valence band. This valence hole recombines with either the photo-electron or a some hole trap. The recombined valence hole and photo-electron forms the self-trapped exciton which eventually emits a photon of LEL. One can, therefore, state that a photon of the HEL band is emitted being accompanied by no more than one photon of the LEL band. It is expected from this argument that the intensity of the HEL band is equal to or larger than that of the LEL band. The experimental result shows that this is the case under the VUV excitation as shown in Fig. 6. Contrary to the VUV excitation, the intensity of the LEL band is stronger than that of the HEL band under the high-energy electron excitation as shown in Figs. 2a and 2b. This enhancement of the LEL band can be explained in terms of the efficient excitation of the valence band due to the delta-ray electrons produced by the incident high-energy electrons. This explanation holds as long as the mean energy of delta-ray electrons is lower than the threshold energy (18 eV) of the $Ba^{++}5p$ band.

4.2.2. BaF_2:MgF_2

The threshold energy of the HEL band (18.0 eV) is proximate to the energy of $Ba^{++}5p$ core exciton (17.1 eV) for the BaF_2 crystal, as shown in Fig. 7. Since there is the same feature of the reflectance spectra observed at the core exciton region in the BaF_2:MgF_2 crystal, one could infer that the first peak at 18.6 eV,

which is located just below the threshold energy (19.3 eV), corresponds to the $Ba^{++}5p$ core exciton. Therefore, the HEL band observed in the BaF_2:MgF_2 crystal can also be interpreted as the AFL due to the radiative recombination of the valence electrons with the $Ba^{++}5p$ holes.

The threshold energy of the BaF_2:MgF_2 crystal locates at the photon energy of 19.3 ± 0.2 eV, which is about 1 eV higher than that of the BaF_2 crystal. The band gap-energy of the BaF_2:MgF_2 crystal determined in the same manner described in the section 4.1 was found to be $E_g = 11.9 \pm 0.4$ eV, which is about 1 eV larger than that of the BaF_2 crystal. This increase in E_g for the BaF_2:MgF_2 crystal probably comes from the larger band gap-energy (14.5 eV) of MgF_2 [34].

The spectrum width of the AFL observed in the BaF_2:MgF_2 crystal is 4.2 ± 0.3 eV, which is larger than that (2.7 ± 0.3 eV) of the BaF_2 crystal. On the basis of the discussion made in the section 4.1 again, this result suggests that the valence band in the BaF_2:MgF_2 crystal is about 1.5 eV wider than that of the BaF_2 crystal. By using photoelectron spectroscopy technique, Poole et al. reported the valence band widths of BaF_2 and MgF_2 to be 3.4 and 6.3 eV, respectively [34]. They have discussed these values in terms of the linear dependence of the total width of the valence band on the distance between the nearest-neighboring atoms in a given crystal. The width of the valence band increases with decreasing the nearest-neighbor distance, which is due to the crystal-field effect associated with the progressive increase of the electron wave-function overlapping in the crystal [34,36]. Since the nearest neighbor distance in BaF_2 and MgF_2 is known to be 2.69 and 1.99 Å respectively [34], the introduction of two moles of MgF_2 into one mol of BaF_2 could result in broadening of the valence band of BaF_2, which is considered to be the responsible mechanism for yielding the luminescence in this newly synthesized crystal.

It is also important to pay attention to the experimental fact that the introduction of the two moles of MgF_2 into one mol of BaF_2 resulted in the decrease in the intensity for the slow component, together with the suppression of the fast component. A difficulty was found in synthesizing such a crystal in which the slow component is highly suppressed without a significant decrease of the fast component intensity, which was one of the goals the present work assigned. However, it can be said that the newly synthesized crystal of BaF_2:MgF_2 manifested the promising enhancement of the fast component at the expense of partially quenching the original luminescence intensity.

The peak appearing at 11.0 eV in the reflectance spectrum as shown in Fig. 7c is attributed to the exciton creation which is 1 eV higher than that of the pure BaF_2 crystal. This increase is due to the increase of E_g for BaF_2:MgF_2 crystal compared to that for BaF_2 crystal. The first peak at 10.0 eV, which is almost the same as that 9.8 eV in BaF_2 crystal, is most likely due to the exciton creation originating from the BaF_2 crystal, which consists in the impurity formed in the crystal.

As can be seen in Fig. 7c the LEL band for the BaF_2:MgF_2 crystal is efficiently excited at excitation photon energy of around 10 eV, but no significant luminescence is observed at excitation photon energy of more than 11 eV. As described just above luminescence at excitation photon energy of around 10 eV corresponds to the creation of excitons in BaF_2, which is the impurity of the BaF_2:MgF_2 crystal. Thus the slow component from the BaF_2:MgF_2 crystal observed in Fig. 2 can be due to the radiative decay of self-trapped excitons formed uniquely from exciton originating from BaF_2 present as impurity in the BaF_2:MgF_2 crystal. It is expected, therefore, that the slow component should be totally suppressed in a perfect BaF_2:MgF_2 crystal.

4.3. CsBr-based crystals

The CsBr crystal has a weak AFL band peaking at 5.3 eV and a dominant luminescence band at 3.2 eV at room temperature, under VUV excitation, as shown in Fig. 10a [4]. The 3.2 eV band observed under the valence band excitation has been considered to be a kind of luminescence associated with defects introduced in the crystal [11].

The 4.5 and the 5.6 eV bands in the CsBr:LiBr crystal confirmed in the present study for the first time, are appearing in the HEL region under VUV excitation, both having the same threshold energy of 14.1 ± 0.1 eV. This value is in good agreement with the transition energy from the outermost-core states of the Cs^+5p to the conduction band [4]. It is, therefore, highly conceivable that these two bands in the CsBr:LiBr crystal are the AFL involving the Br^- 4p valence electrons and the Cs^+5p holes. The 3.5 eV luminescence band observed in the LEL region is considered to be unrelated to the AFL, since this band can also be excited under valence-band excitation as shown in Fig. 10c. Being similar to the case of the CsBr crystal, this luminescence may be interpreted in terms of the luminescence originated from some defects.

At liquid nitrogen temperature three luminescence bands are observed at 5.4, 3.8 and 2.8 eV in the CsBr:LiBr crystal as shown in Fig. 11b. Among these bands the 5.4 eV band has the threshold energy of 14.1 ± 0.1 eV, which can be ascribed to the AFL. The 3.8 and 2.8 eV bands, on the other hand, are effectively excited in the range of the fundamental absorption region. The pure CsBr crystal has also two bands at 3.8 and 2.8 eV at liquid nitrogen temperature, which have been attributed to π emission [11]. Noticing the similarities in the spectroscopic feature observed between

the CsBr and the CsBr:LiBr crystals, one could infer that the π emission mechanism is also responsible to these two bands in the CsBr:LiBr crystal.

Referring to the reflectance spectrum for the CsBr crystal, the first peak (Γ) appearing at 6.70 ± 0.03 eV in the CsBr:LiBr reflection spectrum can be attributed to the exciton creation. It should be stressed here that the peak location has been shifted to the higher energy side by 0.15 eV in the CsBr:LiBr crystal with respect to that in the CsBr crystal, as shown in Fig. 13.

The band gap energy of the CsBr:LiBr crystal has been determined to be 7.5 ± 0.1 eV in the present study, and is clearly larger than that of 7.16 eV of the CsBr crystal [25]. This increase was expected prior to synthesizing the crystal, since E_g of the LiBr crystal is larger than that of the CsBr crystal as described in the section 1.

It is known that the intensity of the AFL from a CsBr crystal at room temperature is about 100 times weaker than that at liquid nitrogen temperature [5,11,37]. According to Davoli et al. [26] this reduction of the intensity at room temperature is attributed to the activation process of the hole to such an energy position in the outermost-core band where the Auger process is highly favoured due to the Urbach effect. Here, the Auger process includes not only the production of an electron–hole pair but the electronic excitation of an exciton, and the excitation or the ionization of defects as well. Since E_g at room temperature is smaller than that at liquid nitrogen temperature [25,36], the Auger process resulting in the non-radiative relaxation of the outermost-core holes proceeds more efficiently at room temperature than at liquid nitrogen temperature.

The most striking feature induced by the introduction of LiBr into CsBr is the enhancement of the AFL intensity. The luminescence intensity in the CsBr:LiBr crystal becomes 40 times larger than that of the CsBr crystal at room temperature. This enhancement can be explained by the mechanism that the Urbach effect [26] in the CsBr:LiBr crystal is suppressed due to the increases in both the band gap-energy and the exciton energy of the CsBr:LiBr crystal. The hole relaxation process through the AFL competing with the Auger process can, therefore, be more efficient in CsBr:LiBr crystal than that in the CsBr crystal, resulting in the intensity enhancement as observed in the CsBr:LiBr crystal.

The decay time measurements carried out in the present study also provide an evidence of the Urbach effect suppression in CsBr:LiBr crystal. Since the suppression is expected to close one of the decay channels of the formation of the Auger process, the apparent decay time should be longer under the suppression of the Urbach effect. The decay time observed in the CsBr:LiBr crystal was 0.90 ± 0.06 ns, which is significantly longer than that (0.20 ± 0.05 ns) in the CsBr crystal as expected.

The AFL spectra of the CsBr:LiBr crystal have peaks around 5.6 and 4.3 eV as shown in Figs. 8b and 10b. The intensity of the 5.6 eV band is about twice as intense as that of the 4.3 eV band under VUV excitation. On the contrary, the intensity of the 5.6 eV band is about 80 times weaker than that of the 4.3 eV band under the high-energy electron excitation. This reduction in the intensity of the 5.6 eV band can probably be explained by the self-absorption of the ~ 5.6 eV photons in the crystal. Since the absorption length for 511 keV annihilation radiation is about 10 cm, outermost-core holes are produced almost uniformly over the crystal volume under the high-energy electron excitation. The photons with an energy of ~ 5.6 eV emitted in the bulk of the crystal, could be strongly absorbed due to the opacity, resulting in low luminescence intensity. The outermost-core holes are on the other hand, produced within $\sim 10^{-6}$ cm from the crystal surface under the VUV excitation. These photons are, therefore, free from the self-absorption, and are detected as a strong emission. It is anticipated that a good optical transmission of the crystal can improve the luminescence intensity of the 5.6 eV band.

As Fig. 8a displays, the emission band observed in the CsBr crystal distributes from 3.2 to 6.6 eV. The maximum energy (6.6 eV) is in good agreement with the values reported so far [3,4]. As can be seen in Table 5, however, the minimum energy measured is about 1 eV lower than those reported in refs. [3,4], and its spectrum width determined 3.4 eV is about 1.5 eV larger than those reported in refs. [3,4]. It should be noted that the emission spectrum is obtained by employing the time-resolved spectroscopy in this work [38]. By using the valence band widths ΔE_v^p, which are deduced from the photoelectron spectroscopy [36,39], the expected location of luminescence in the CsBr crystal can be calculated to be either from 4.3 to 7.3 eV or from 4.5 to 6.6 eV depending upon the numerical values of ΔE_v^p to be used, i.e. 3.0 eV [36] or 2.1 eV [39]. Accurate measurements of the valence band width are needed to compare the measured spectrum width measured in the present study and the calculated one.

5. Conclusion

It has been demonstrated that the introduction of such foreign species of SrF_2 and MgF_2 into BaF_2 results in the significant suppression of the slow component luminescence. Although the decrease of the fast component is also induced, the suppression of the slow component is more effective than that of the fast component. The Sr^{++} and Mg^{++} ions act as electron trapping centers, preventing the formation of self-

trapped excitons by electron–hole pair. The suppression technique of the slow component provides a promising way of developing new scintillation material suitable for high counting rate experiments.

Detailed study on the fast component appearing in the newly synthesized BaF_2-based crystals, the BaF_2:Sr and BaF_2:MgF_2 crystals open a way of investigating the band structure in this type of the crystals by combining them with the AFL measurements presented in this work. While the introduction of the Sr^{++} ions yielded no significant difference in the band structure of BaF_2 crystal, an appreciable difference is observed in the band structure of the BaF_2:MgF_2 crystal compared to that of the BaF_2 crystal.

It has also been shown that the luminescence intensity of the CsBr:LiBr crystal at room temperature is 40 times more intense than that of the CsBr crystal. This enhancement is attributed to the suppression of the Urbach effect due to increases in the band-gap energy and in the exciton energy of the CsBr:LiBr crystal compared with those in the CsBr crystal. At liquid nitrogen temperature, the increase of the luminescence intensity in the CsBr:LiBr crystal is less effective, being only twice more intense than that of the CsBr crystal. The increase in the decay time for the CsBr:LiBr crystal also provides an evidence to the suppression of the Urbach effect in this crystal.

Acknowledgements

The author would like to express her sincere gratitude to Rikkyo University for the fellowship and facilities offered, and to Instituto de Pesquisas Energéticas e Nucleares – IPEN-CNEN/SP for opportunity and support given to make research in Japan, which made possible to carry out this work. She would like to thank to Prof. S. Kubota for his suggestions and discussions during the course of this work. She is grateful to Prof. J. Ruan (Gen) for his useful suggestions and careful reading of the manuscript and Prof. F. Shiraishi for his encouragement and guidance in the experiments performed at Institute for Atomic Energy, Rikkyo University. She is also very grateful to Mr. N. Nunoya and Mr. Y. Ando for their invaluable advice during the course of this work. She would like to thank to Dr. S. Sakuragui, Union Material Inc., for offering the BaF_2-based crystals and for his useful guidance and attention in the crystal growth. She wishes to acknowledge her indebtedness to Dr. M. Suzuki, RIKKEN, and Dr. M. Ithoh, Shinshu University, for their valuable advice and careful reading of the manuscript. She is pleased to acknowledge the hospitality and friendship of the member staffs of the Group of Nuclear and Radiation Physics, Department of Physics, Rikkyo University. The experiments made with VUV photons were carried out at Synchrotron Orbital Radiation Facility, Institute for Solid State Physics, Tokyo University and the support of the staff is gratefully acknowledged.

References

[1] Yu. M. Aleksandrov, V.N. Makhov, P.A. Rodnyi, T.I. Syreishchikova and M.N. Yakimenko, Sov. Phys. Solid State 26 (1984) 1734.
[2] Yu. M. Aleksandrov, V.N. Makhov, N M. Khaiduko and M N. Yakimenko, Sov. Phys. Solid State 31 (1989) 1609.
[3] J.L. Jansons, V.L. Krumins, Z.A. Rachiko and J.A. Valbis, Phys. Status Solidı 144 (1987) 835.
[4] S. Kubota, M. Itoh, J. Ruan, S. Sakuragui and S. Hashimoto, Phys Rev. Lett. 60 (1988), 2319.
[5] S. Kubota, J. Ruan, M. Itoh, S. Hashimoto and S. Sakuragui, Nucl. Instr. and Meth. A 289 (1990) 253.
[6] S. Kubota, N. Kanai and J. Ruan, Phys. Status Solidi 139 (1987) 635.
[7] S. Kubota, in: Vacuum Ultravıolet Radiatıon Physıcs, Proc. 10th VUV Conf eds. F.J. Wuilleumier, Y. Poroff and I. Nenner, Paris, 1992 (World Scientific) p 511
[8] E.N. Mel'chacov, P.A. Rodnyl, B.V. Rybakov, A. Ya. Smakov and M.A. Terekhin, Sov. Phys. Solid State 31 (1989) 878.
[9] V.N. Makhov, Nucl. Instr. and Meth. A 308 (1991) 187.
[10] M. Itoh, S. Hashimoto, S Sakuragui and S. Kubota, Solid State Commun. 65 (1988) 523.
[11] M. Itoh, S. Kubota, J Ruan and S. Hashimoto, Rev. Sol. State Scıence 4 (1990) 337.
[12] M. Itoh and H. Itoh, Phys. Rev. B 46 (1992) 15609.
[13] P.A. Rodnyı and M.A Terekhin, Phys. Status Solıdi 283 (1991) 283.
[14] M. Murashıta, H. Satoh, K. Tobimatsu, M. Chiba, T. Hırose and F. Takashi, Nucl. Instr. and Meth. A 243 (1986) 67
[15] C.L. Woody and D.F. Anderson, Nucl. Instr. and Meth. A 265 (1988) 291.
[16] P. Schotanus, C.W.E. Van Eıjk, R.W. Hollander and J. Pijpelink, IEEE Trans. Nucl. Sci NS-34 (1987) 272.
[17] P. Schotanus, P. Dorenbos, C.W.E. Van Eijk and H.J. Lamfers, Nucl. Instr and Meth. A 281 (1989) 162.
[18] P. Schotanus, P. Dorenbos, C.W.E. Van Eıjk and R W. Hollander, IEEE Trans. Nucl Sci. NS-36 (1989) 132.
[19] C.L. Woody, P.W Levy and J.A Kıerstead, IEEE Trans. Nucl. Sci. NS-36 (1989) 536.
[20] P. Derenbos, R. Vısser, C.W.E. van Eijk, J. Valbis and N.M. Khaidukov, IEEE Trans. Nucl. Sci. NS-39 (1992) 506.
[21] A.V. Golovin, E.N. Mel'chakov, V.V. Mikhaılin, P.A. Rodnyl and M.A. Terekhin, Sov. Phys. Solıd State 32 (1989) 692.
[22] P.A. Rodnyi, M.A. Terekhın and E.N. Mel'chakov, J. Lumın. 47 (1991) 275.
[23] Yu. M. Aleksandrov, I.L. Kuusmann, V.N. Makhov, S.B. Mirov, T.V. Uvarova and M N. Yakımenko, Nucl. Instr. and Meth. A 308 (1991) 208.
[24] R. Visser, P. Dorenbos, C.W.E. van Ejik, R.W. Hollander and P. Schotanus, Trans. Nucl. Sci. NS-38 (1991) 178.

[25] I. Kuusmann, T. Kloiber, W. Laasch and G. Zimmerer, Proc. 6th Europhysical Topical Conf., Latice Defects in Ionic Material, LATDIM-90, Radiat. Eff. and Def. in Solids 119–121 (1991) 21.
[26] I. Davoli, V.V. Mikhailin, S. Stizza and A.N. Vasil'ev, J. Lumin. 51 (1992) 275.
[27] F.C. Brown, C. Gähuiller and H. Fujita, Phys. Rev. B 2 (1970) 2126.
[28] E.M. Levin, C.R. Robbins and H.F. McMurdie, In: Phase Diagrams for Ceramists (American Ceramic Society Inc., 1964) p. 428.
[29] E.M. Levin, C.R. Robbins and H.F. McMurdie, in: Phase Diagrams for Ceramists (National Bureau of Standards, 1969) p. 268.
[30] The peak at 195 nm is not resolved because of the limited sensitivity of the present detection system in the spectral region above 6.7 eV.
[31] G.W. Rubloff, Phys. Rev. B 5 (1972) 662.
[32] Y. Onodera, M. Okazaki and T. Inui, J. Phys. Soc. Jpn. 21 (1966) 2229.
[33] A.B. Kunz, Phys. Rev. 175 (1968) 1147.
[34] R.T. Poole, J. Szajman, R.C.G. Leckey, J.G. Jenkin and J. Liesegang, Phys. Rev. B 12 (1975) 5872.
[35] M.N. Kabler, R.T. Willians, Phys. Rev. B 18 (1976) 725.
[36] R.T. Poole, J.G. Jenkin, J. Liesegang and R.C.G. Leckey, Phys. Rev. B 11 (1975) 5179.
[37] Yu. M. Aleksandrov, V.N. Makhov, T.I. Syrejshchikova and M.N. Yakimenko, Nucl. Instr. and Meth. A 261 (1987) 153.
[38] In ref. [4], the emission spectrum for AFL is obtained by subtracting the spectrum under the excitation of valence band from the spectrum under outermost-core band excitation, by assuming that the low-energy luminescence spectrum under the outermost-core band excitation is the same as that under the valence band excitation.
[39] J.A. Smith and W. Pong, Phys. Rev. B 12 (1975) 5931.
[40] T. Tominiki and T. Miyata, J. Phys. Soc. Japan 27 (1969) 658.
[41] W. Pong, G.S. Inoye and S.K. Okada, Phys. Rev. B 18 (1978), 4422.